RESEARCH PAPER

Formulation and Mechanistic Evaluation of Andrographolide-Loaded Nano-Structured Hydrogel for Enhanced Angiogenic and Anti-Inflammatory Activity in Diabetic Foot Ulcer Management

[1] Y. Ganesh Kumar, [2] Jaymala Arun Kumawat, [3*] Landge Dhananjay Ashok, [4] Pavithra S, [5] Nishant Singh Katiyar, [6] Saranya Punniyakotti, [7] Amrita Thakur, [8] Diksha Sharma

[1]Associate Professor, Department of Pharmaceutics, Bharat Institute of Pharmacy, Mangalpally (V), Ibrahimpatnam (M), R.R. Dist - 501510, Telangana.

[2]Assistant Professor, Vishwakarma University, School of Pharmacy, Kondwa, Pune, Maharashtra, 411048.

[3*]Research Scholar, Gautam College of Pharmacy, Hamirpur, Himachal Pradesh, 177001.

Email: dhananjaylandge33@gmail.com

[4]Research Scholar, Department of Pharmacy Practice, Saveetha College of Pharmacy, Saveetha Institute of Medical and Technical Sciences (SIMATS), Saveetha Nagar, Thandalam, Chennai, Tamil Nadu - 602105, India. Orchid id: 0009-0006-1491-6708

[5]Professor, School of Pharmacy, Mangalayatan University, Aligarh, Uttar Pradesh, 202146.

[6]Professor, Department of Pharmacy Practice, Saveetha College of Pharmacy, Saveetha Institute of Medical and Technical Sciences (SIMATS), Saveetha Nagar, Thandalam, Chennai, Tamil Nadu - 602105, India. Orchid id: 0000-0003-0802-7999

[7]Assistant Professor, School of Pharmacy, Vishwakarma University, Pune, Maharashtra.

[8]Assistant Professor, Rayat Bahra University, Mohali, Punjab, 140104.

*Corresponding Author: Landge Dhananjay Ashok**

Abstract

Diabetic foot ulcers (DFUs) are chronic non-healing wounds characterized by persistent inflammation, impaired angiogenesis, and delayed tissue regeneration. The present study aimed to develop and mechanistically evaluate an andrographolide-loaded nano-structured hydrogel (AG-NSH) for enhanced anti-inflammatory and pro-angiogenic activity in DFU management. Andrographolide, a bioactive diterpenoid from *Andrographis paniculata*, was incorporated into an oil-in-water nanoemulsion and subsequently embedded within a chitosan–Carbopol hydrogel matrix. The optimized nanoemulsion exhibited a mean particle size of 128.4 ± 6.3 nm, polydispersity index of 0.214 ± 0.02, zeta potential of −28.6 ± 1.9 mV, and entrapment efficiency of 87.2 ± 2.4%. The hydrogel demonstrated suitable pH (5.82 ± 0.12), pseudoplastic rheological behavior, and sustained drug release up to 48 hours following anomalous diffusion kinetics. Ex vivo studies confirmed enhanced dermal permeation with controlled flux. In vitro biological evaluation showed >85% cell viability in human dermal fibroblasts and keratinocytes. AG-NSH significantly reduced TNF-α, IL-6, and COX-2 expression while restoring VEGF secretion and endothelial tube formation under hyperglycemic conditions. The dual anti-inflammatory and angiogenic modulation suggests that AG-NSH may offer a promising localized therapeutic approach for diabetic foot ulcer treatment.

Keywords: Andrographolide; Nano-structured hydrogel; Diabetic foot ulcer; Anti-inflammatory activity; Angiogenesis; Sustained release.

How to cite this article: Kumar YG, Kumawat JA, Ashok LD, Pavithra S, Katiyar NS, Punniyakotti S, Thakur A, Sharma D. Formulation and Mechanistic Evaluation of Andrographolide-Loaded Nano-Structured Hydrogel for Enhanced Angiogenic and Anti-Inflammatory Activity in Diabetic Foot Ulcer Management. Int J Drug Deliv Technol. 2026;16(10s): 819-837; DOI: 10.25258/ijddt.16.10s.97

1. Introduction

Diabetic foot ulcer (DFU) represents one of the most severe and economically burdensome complications of diabetes mellitus. It is estimated that approximately 15–25% of individuals with diabetes develop foot ulcers during their lifetime, with a substantial proportion progressing to infection, hospitalization, and lower limb amputation. The pathogenesis of DFU is multifactorial, involving peripheral neuropathy, microvascular dysfunction, impaired immune response, and chronic inflammation. Persistent hyperglycaemia induces oxidative stress, endothelial damage, and dysregulated cytokine production, collectively disrupting the tightly regulated phases of wound healing. Unlike acute wounds that progress sequentially through hemostasis, inflammation, proliferation, and remodelling, diabetic wounds often remain trapped in a prolonged inflammatory state, resulting in delayed granulation tissue formation and insufficient re-epithelialization (Bhattacharya *et al.*, 2026; Chan *et al.*, 2026; Lázaro-Martínez *et al.*, 2026; Mahmoud *et al.*, 2026; Mariani *et al.*, 2026; Meloni *et al.*, 2026).

Chronic inflammation is a hallmark feature of DFU. Elevated levels of pro-inflammatory cytokines such as tumour necrosis factor-alpha (TNF-α), interleukin-6 (IL-6), and cyclooxygenase-2 (COX-2) contribute to sustained tissue

damage and impaired fibroblast function. Excessive activation of nuclear factor kappa B (NF-κB) signalling further perpetuates inflammatory cascades, preventing the transition toward the proliferative phase of healing. Simultaneously, diabetic conditions impair angiogenesis, leading to inadequate oxygen and nutrient supply to regenerating tissues. Vascular endothelial growth factor (VEGF), a key mediator of neovascularization, is often downregulated under hyperglycaemic and oxidative stress conditions. The combined presence of persistent inflammation and insufficient angiogenesis creates a hostile wound microenvironment that delays healing and increases susceptibility to infection (Gao *et al.*, 2025; Lee *et al.*, 2025; Lin *et al.*, 2025; H. Liu, X. Xiang*, et al.*, 2025; H. Liu, S. Zhao*, et al.*, 2025).

Current treatment strategies for DFU primarily involve debridement, infection control, pressure off-loading, and application of topical dressings. While these approaches provide supportive care, they often fail to directly modulate underlying molecular abnormalities. Conventional topical anti-inflammatory agents may reduce inflammation temporarily but lack sustained release characteristics and do not adequately stimulate angiogenesis. Furthermore, poor drug solubility and limited dermal penetration reduce therapeutic efficacy. Therefore, there is a compelling need for advanced delivery systems capable of addressing multiple pathological mechanisms simultaneously while ensuring localized and controlled drug release (Han, 2025; Hanley & Manna, 2025; Jiao *et al.*, 2025; Leme *et al.*, 2025; Liu & Yu, 2025; Y. Liu *et al.*, 2025; Z. Liu *et al.*, 2025; Lu *et al.*, 2025).

Andrographolide, a diterpenoid lactone isolated from *Andrographis paniculata* (Burm. f.) Wall. ex Nees, has attracted attention due to its potent anti-inflammatory, antioxidant, and immunomodulatory properties. Previous studies have demonstrated that andrographolide inhibits NF-κB activation, suppresses TNF-α and IL-6 production, and downregulates COX-2 expression. In addition to its anti-inflammatory effects, andrographolide has been reported to promote angiogenic signalling through modulation of VEGF and PI3K/Akt pathways. These dual pharmacological properties make it a promising candidate for DFU management. However, its clinical application is limited by poor aqueous solubility, low bioavailability, and rapid metabolic degradation (Han *et al.*, 2023; Huang *et al.*, 2023; Indirapriyadarshini *et al.*, 2023; Jain & Sudandiradoss, 2023; Jiaqi *et al.*, 2023; Yang *et al.*, 2022; Yu *et al.*, 2022; Yuan *et al.*, 2022).

Nanotechnology-based drug delivery systems offer a promising solution to these challenges. Nanoemulsions, characterized by droplet sizes typically below 200 nm, enhance solubilization of lipophilic compounds and improve dermal penetration through increased surface area and interaction with skin lipids. Incorporation of nanoemulsions into hydrogel matrices further enhances therapeutic potential by providing sustained release, prolonged residence time, and maintenance of a moist wound environment conducive to healing. Hydrogels composed of biocompatible polymers such as chitosan and Carbopol not only serve as drug carriers but also contribute to wound healing through bioadhesion, antimicrobial activity, and structural support (Alanazi & Ben Said, 2022; Elsheikh *et al.*, 2021; Huang *et al.*, 2022; Li *et al.*, 2022; Ramadani *et al.*, 2021; Shrivastava & Kaur, 2023; Zhou *et al.*, 2023).

The present study was therefore designed to formulate and evaluate an andrographolide-loaded nano-structured hydrogel (AG-NSH) aimed at enhancing localized delivery, suppressing chronic inflammation, and restoring angiogenic balance in diabetic wound conditions. By integrating nanoemulsion technology with a bioadhesive hydrogel system, the formulation sought to overcome solubility limitations, improve dermal permeation, and provide sustained therapeutic action. The investigation further aimed to elucidate the mechanistic basis of its anti-inflammatory and pro-angiogenic effects using in vitro cellular models relevant to diabetic foot ulcer pathology.

2. Materials and Methods

2.1 Materials

Andrographolide (≥98% purity), a bioactive diterpenoid lactone isolated from *Andrographis paniculata* (Burm. f.) Wall. ex Nees, was procured from a certified phytochemical supplier and authenticated by high-performance liquid chromatography prior to formulation development. The compound was stored in airtight amber containers at 4 ± 1 °C to prevent photolytic and oxidative degradation throughout the study. Capryol 90, isopropyl myristate (IPM), and oleic acid were screened as potential oil phases based on their biocompatibility and solubilization capacity. Tween 80 (polysorbate 80) and Span 20 were evaluated as surfactants owing to their established safety profile in topical formulations. Polyethylene glycol 400 (PEG 400) and propylene glycol were assessed as co-surfactants to enhance interfacial flexibility and nanoemulsion stability. Chitosan (medium molecular weight, degree of deacetylation ≥85%) was selected for its intrinsic wound healing, antimicrobial, and bioadhesive properties. Carbopol 934P was used as a secondary polymer to impart structural strength and viscosity control. Glacial acetic acid, triethanolamine, methanol, phosphate-buffered saline (PBS, pH 7.4), and other reagents were of analytical grade. Human dermal fibroblast (HDF) cells and HaCaT keratinocyte cell lines were obtained from a recognized cell repository and maintained under sterile culture conditions in Dulbecco's Modified Eagle Medium supplemented with 10% fetal bovine serum and 1% antibiotic solution. ELISA kits for TNF-α, IL-6, COX-2, and VEGF

quantification were procured from validated biotechnology suppliers. All biological reagents were of cell-culture grade.

2.2 Preformulation Studies

2.2.1 Solubility Analysis

The solubility of andrographolide in various formulation components was systematically evaluated to identify the most suitable oil phase and surfactant system for nanoemulsion development. Since andrographolide exhibits poor aqueous solubility and moderate lipophilicity, optimization of the solvent environment was considered critical for achieving high entrapment efficiency and sustained drug release. An excess quantity of andrographolide was added to 2 mL of each selected oil, surfactant, and co-surfactant in sealed borosilicate vials. The mixtures were vortexed for uniform dispersion and subsequently placed in an orbital shaker maintained at 37 ± 1 °C for 72 hours to ensure equilibrium solubilization. After equilibration, samples were centrifuged at 10,000 rpm for 15 minutes to separate undissolved drug. The supernatant was carefully collected, filtered through a 0.22 µm membrane filter, and diluted appropriately with methanol. Drug concentration was quantified using UV–visible spectrophotometry at λmax 223 nm after calibration curve validation. Solubility values were expressed in mg/mL. The oil phase demonstrating the highest solubilization capacity was selected for nanoemulsion preparation, as enhanced drug solubility within the oil core directly influences encapsulation efficiency and formulation stability (Kulsirirat *et al.*, 2021; Lapmanee *et al.*, 2025; Talodthaisong *et al.*, 2023; Ye *et al.*, 2026; Zhou *et al.*, 2023).

2.2.2 Drug–Excipient Compatibility (FTIR)

Fourier-transform infrared spectroscopy (FTIR) was performed to evaluate potential physicochemical interactions between andrographolide and selected excipients. Compatibility assessment was essential to ensure chemical stability during processing and storage. Pure andrographolide, individual polymers (chitosan and Carbopol 934P), and their physical mixtures (1:1 w/w) were analyzed using the potassium bromide (KBr) pellet technique. Approximately 2 mg of sample was mixed with dry KBr powder, compressed into transparent discs, and scanned over a spectral range of 4000–400 cm^{-1} using an FTIR spectrophotometer.

Characteristic functional group peaks of andrographolide were carefully examined, including:

- O–H stretching (~3400 cm^{-1})
- C=O stretching of lactone (~1725 cm^{-1})
- C=C stretching (~1640 cm^{-1})
- C–O stretching (~1100–1200 cm^{-1})

Spectra obtained from physical mixtures were compared to those of pure drug. The absence of peak disappearance, broadening, or significant shifts indicated that no chemical interaction occurred between andrographolide and selected polymers, confirming compatibility within the hydrogel matrix (Kulsirirat *et al.*, 2021; Lapmanee *et al.*, 2025; Talodthaisong *et al.*, 2023; Ye *et al.*, 2026; Zhou *et al.*, 2023).

2.3 Preparation of Andrographolide Nanoemulsion

The nanoemulsion was developed to enhance the solubility, stability, and dermal penetration of andrographolide, which inherently exhibits limited aqueous solubility and moderate permeability. The formulation strategy was designed to produce a stable oil-in-water (O/W) nanoemulsion with nanoscale droplet distribution to facilitate improved drug diffusion through the stratum corneum and sustained release within the wound microenvironment (Kulsirirat *et al.*, 2021; Lapmanee *et al.*, 2025; Talodthaisong *et al.*, 2023; Ye *et al.*, 2026; Zhou *et al.*, 2023).

2.3.1 Selection of Oil, Surfactant, and Co-surfactant

Selection of formulation components was based on solubility data, physicochemical compatibility, and dermal safety considerations. Capryol 90 demonstrated superior solubilization capacity for andrographolide among the tested oils and was therefore selected as the oil phase. The relatively medium-chain lipid nature of Capryol 90 was considered advantageous for enhancing dermal absorption due to its permeation-enhancing properties (Kulsirirat *et al.*, 2021; Lapmanee *et al.*, 2025; Talodthaisong *et al.*, 2023; Ye *et al.*, 2026; Zhou *et al.*, 2023). Tween 80 was selected as the primary surfactant owing to its high hydrophilic–lipophilic balance (HLB ~15), which favors formation of oil-in-water nanoemulsions. Additionally, Tween 80 possesses good dermatological tolerance and has been widely used in topical nanoformulations. PEG 400 was chosen as the co-surfactant because of its ability to reduce interfacial tension further and improve the flexibility of the interfacial film, thereby facilitating the formation of smaller droplet sizes. The selection criteria also included non-irritancy, regulatory acceptance for topical application, and compatibility with hydrogel polymers (Kulsirirat *et al.*, 2021; Lapmanee *et al.*, 2025; Lu *et al.*, 2026; Prasathkumar & Sadhasivam, 2021).

2.3.2 Construction of Pseudo-Ternary Phase Diagram

To determine the optimal composition range capable of forming a stable nanoemulsion, pseudo-ternary phase diagrams were constructed using the aqueous titration method. This approach enabled identification of the nanoemulsion region based on visual transparency and isotropy. Surfactant and co-surfactant were mixed in predetermined ratios (Smix ratios of 1:1, 2:1, and 3:1). Each Smix ratio was blended with the selected oil phase in varying weight proportions ranging from 1:9 to 9:1. Distilled water was added dropwise under continuous magnetic stirring at ambient temperature. After each addition, the mixture was visually inspected for clarity and homogeneity. The point at which turbidity or phase separation occurred was recorded. Transparent, low-viscosity, and isotropic systems were classified as nanoemulsion regions. These compositions were

mapped on triangular coordinate graphs to delineate the nanoemulsion zone. The Smix ratio that generated the widest nanoemulsion region and demonstrated rapid self-emulsification without phase instability was selected for final formulation preparation (Kulsirirat *et al.*, 2021; Lapmanee *et al.*, 2025; Lu *et al.*, 2026; Prasathkumar & Sadhasivam, 2021).

2.3.3 Preparation Method

The optimized nanoemulsion was prepared using high-speed homogenization followed by probe sonication to achieve nanoscale droplet distribution. Initially, andrographolide was dissolved in the selected oil phase under gentle magnetic stirring at 40 °C to ensure complete solubilization. The pre-mixed surfactant–co-surfactant blend (Smix) was then gradually added to the oil phase while maintaining continuous stirring to form a uniform pre-concentrate. Distilled water was incorporated slowly under high-speed homogenization at 12,000–15,000 rpm for 10 minutes to form a coarse emulsion. Subsequently, the coarse emulsion was subjected to probe sonication for 5 minutes using pulsed cycles (30 seconds on, 10 seconds off) to minimize thermal degradation and reduce droplet size. The resulting nanoemulsion was allowed to equilibrate at room temperature and visually examined for transparency, homogeneity, and absence of phase separation. The formulation was stored in airtight glass containers for further characterization. The underlying mechanism of droplet size reduction was attributed to the combined effects of mechanical shear forces and acoustic cavitation generated during sonication. These forces disrupted larger droplets into nanoscale structures while surfactant molecules stabilized the newly formed interfaces, preventing coalescence (Kulsirirat *et al.*, 2021; Lapmanee *et al.*, 2025; Lu *et al.*, 2026; Prasathkumar & Sadhasivam, 2021).

2.4 Characterization of Nanoemulsion

Comprehensive physicochemical characterization of the developed andrographolide nanoemulsion was performed to evaluate droplet size distribution, colloidal stability, drug encapsulation efficiency, and morphological characteristics. These parameters were critical to ensure formulation uniformity, stability during storage, and enhanced dermal delivery performance.

2.4.1 Particle Size and Polydispersity Index

The mean droplet size and polydispersity index (PDI) of the nanoemulsion were determined using dynamic light scattering (DLS) based on photon correlation spectroscopy. Measurements were performed using a Malvern Zetasizer at 25 ± 0.5 °C. Prior to analysis, the nanoemulsion sample was diluted 1:100 with filtered distilled water to prevent multiple scattering effects and to ensure accurate particle size measurement. The refractive index of the dispersed phase and viscosity of the medium were entered into the instrument software according to manufacturer specifications. The average hydrodynamic diameter (z-average) was recorded in nanometers, and PDI values were obtained as a measure of size distribution uniformity. A PDI value below 0.3 was considered indicative of a narrow size distribution and homogenous droplet population.

Each measurement was performed in triplicate, and results were expressed as mean ± standard deviation. Small droplet size was considered essential for enhancing surface area, improving dermal penetration, and ensuring sustained release of andrographolide within the wound microenvironment (Kulsirirat *et al.*, 2021; Lapmanee *et al.*, 2025; Lu *et al.*, 2026; Prasathkumar & Sadhasivam, 2021).

2.4.2 Zeta Potential

Zeta potential analysis was conducted to assess the electrostatic stability of the nanoemulsion system. Measurements were carried out using electrophoretic light scattering on the same instrument. The nanoemulsion sample was diluted appropriately with distilled water and transferred into a folded capillary cell. The electrophoretic mobility of droplets was measured under an applied electric field, and zeta potential values were calculated using the Smoluchowski equation. Zeta potential values greater than ±25 mV were considered indicative of sufficient electrostatic repulsion to prevent droplet aggregation. Stable surface charge was particularly important for maintaining long-term dispersion stability and preventing coalescence during storage (Kulsirirat *et al.*, 2021; Lapmanee *et al.*, 2025; Lu *et al.*, 2026; Prasathkumar & Sadhasivam, 2021).

2.4.3 Entrapment Efficiency

Entrapment efficiency (EE%) was determined to quantify the proportion of andrographolide successfully encapsulated within the nanoemulsion droplets. The nanoemulsion was subjected to ultracentrifugation at 20,000 rpm for 30 minutes at 4 °C. The supernatant containing free (unencapsulated) drug was carefully separated and filtered. The concentration of free andrographolide was quantified using UV–visible spectrophotometry at 223 nm after suitable dilution with methanol. Entrapment efficiency was calculated using the formula (Kulsirirat *et al.*, 2021; Lapmanee *et al.*, 2025; Lu *et al.*, 2026; Prasathkumar & Sadhasivam, 2021):

$$EE\ (\%) = (\text{Total Drug} - \text{Free Drug}) / \text{Total Drug} \times 100$$

High entrapment efficiency was considered essential to ensure adequate drug loading, minimize drug wastage, and maintain prolonged therapeutic activity at the wound site.

2.4.4 Transmission Electron Microscopy (TEM)

The morphological characteristics and structural integrity of nanoemulsion droplets were evaluated using transmission electron microscopy (TEM). A small volume of diluted nanoemulsion was placed onto a carbon-coated copper grid and allowed to adsorb for 2 minutes. Excess liquid was removed using filter paper. The sample was negatively stained with 1% phosphotungstic acid to enhance contrast and then

air-dried at room temperature. The grids were examined under TEM at appropriate magnifications. Droplet shape, surface smoothness, and size distribution were visually assessed. Spherical morphology with uniform distribution was considered indicative of successful nanoemulsion formation. TEM analysis provided complementary confirmation of particle size findings obtained from DLS and allowed visualization of nanoscale architecture (Kulsirirat *et al.*, 2021; Lapmanee *et al.*, 2025; Lu *et al.*, 2026; Prasathkumar & Sadhasivam, 2021).

2.5 Formulation of Nano-Structured Hydrogel

The nano-structured hydrogel was developed as a dual-function delivery platform capable of providing sustained drug release, enhanced dermal retention, and a moist wound healing environment. The hydrogel matrix was designed to combine the bioadhesive and intrinsic wound-healing properties of chitosan with the viscosity-modulating and structural reinforcement capability of Carbopol 934P (Kulsirirat *et al.*, 2021; Lapmanee *et al.*, 2025; Lu *et al.*, 2026; Prasathkumar & Sadhasivam, 2021).

2.5.1 Selection of Polymer Matrix (Chitosan–Carbopol System)

Chitosan was selected as the primary polymer due to its biocompatibility, biodegradability, hemostatic activity, and intrinsic antimicrobial effects. Additionally, chitosan possesses a positive surface charge in mildly acidic conditions, which facilitates interaction with negatively charged cell membranes and enhances tissue adhesion. These characteristics were considered particularly advantageous for diabetic wounds, where microbial colonization and delayed epithelialization are common. Carbopol 934P was incorporated as a secondary polymer to improve mechanical strength, viscosity, and gel consistency. Carbopol forms a three-dimensional crosslinked network upon neutralization, enabling entrapment of the nanoemulsion droplets within the hydrogel matrix. Chitosan (1% w/v) was dissolved in 1% v/v glacial acetic acid under continuous magnetic stirring for 6 hours until a clear solution was obtained. Carbopol 934P (0.5% w/v) was separately dispersed in distilled water and allowed to hydrate overnight to ensure complete swelling and uniform polymer dispersion. The two polymer solutions were then blended under slow mechanical stirring to obtain a homogeneous gel base. The interaction between protonated amino groups of chitosan and carboxyl groups of Carbopol contributed to the formation of a semi-interpenetrating polymer network, enhancing gel stability and mucoadhesive properties (Kulsirirat *et al.*, 2021; Lapmanee *et al.*, 2025; Lu *et al.*, 2026; Prasathkumar & Sadhasivam, 2021).

2.5.2 Incorporation of Nanoemulsion

The optimized andrographolide nanoemulsion was incorporated into the hydrated polymer matrix under controlled stirring conditions to ensure uniform distribution without destabilizing the nanoscale droplets. The nanoemulsion was added gradually to the chitosan–Carbopol gel base while stirring at 500 rpm to avoid air entrapment. Triethanolamine was added dropwise to neutralize the Carbopol component and adjust the pH of the formulation to a physiologically acceptable range (5.5–6.5), suitable for topical application and compatible with the slightly acidic wound environment. Homogeneity was ensured through gentle stirring for an additional 20 minutes. The final formulation was visually inspected for uniformity, absence of phase separation, and smooth texture. Entrapment of nanoemulsion droplets within the polymeric network was expected to reduce droplet mobility, thereby providing sustained release of andrographolide while maintaining localized drug concentration at the wound site (Kulsirirat *et al.*, 2021; Lapmanee *et al.*, 2025; Lu *et al.*, 2026; Prasathkumar & Sadhasivam, 2021).

2.5.3 pH and Rheological Evaluation

The pH of the developed nano-structured hydrogel was measured using a calibrated digital pH meter. Approximately 1 g of hydrogel was dispersed in 10 mL of distilled water and allowed to equilibrate before measurement. Maintaining a pH close to physiological skin pH was essential to prevent irritation and ensure patient compliance. Rheological behaviour was evaluated using a Brookfield viscometer equipped with appropriate spindle geometry. Measurements were conducted at varying rotational speeds to determine flow characteristics and shear-thinning behaviour. The formulation was assessed for pseudoplastic flow, which is desirable for topical preparations. Pseudoplastic systems exhibit decreased viscosity under shear stress (during spreading) and regain viscosity upon removal of stress, ensuring adequate residence time at the application site. The viscosity profile also provided insight into the structural integrity of the polymer network and its ability to retain nanoemulsion droplets without sedimentation (Kulsirirat *et al.*, 2021; Lapmanee *et al.*, 2025; Lu *et al.*, 2026; Prasathkumar & Sadhasivam, 2021).

2.6 *In Vitro* Drug Release Study

The in vitro drug release profile of andrographolide from the nano-structured hydrogel was evaluated to determine the release kinetics, diffusion behaviour, and sustained delivery potential of the formulation. Sustained and controlled drug release was considered critical for diabetic foot ulcer management, as prolonged local exposure to anti-inflammatory and pro-angiogenic agents supports tissue regeneration and reduces repeated application frequency. Drug release studies were performed using a vertical Franz diffusion cell apparatus with an effective diffusion area of approximately 2.5 cm^2. A dialysis membrane (molecular weight cut-off 12,000–14,000 Da) was soaked overnight in phosphate-buffered saline (PBS, pH 7.4) prior to mounting. The hydrated membrane was carefully clamped between the

donor and receptor compartments, ensuring no air bubbles were trapped. The receptor compartment was filled with PBS (pH 7.4) containing 0.5% v/v Tween 80 to maintain sink conditions for andrographolide, which exhibits limited aqueous solubility. The receptor medium was maintained at 37 ± 0.5 °C using a circulating water bath and stirred continuously at 600 rpm using a magnetic stirrer to simulate physiological conditions (Kulsirirat *et al.*, 2021; Lapmanee *et al.*, 2025; Lu *et al.*, 2026; Prasathkumar & Sadhasivam, 2021). Approximately 1 g of nano-structured hydrogel containing a predetermined quantity of andrographolide was uniformly applied to the donor compartment. At predetermined time intervals (0.5, 1, 2, 4, 6, 8, 12, 24, 36, and 48 hours), 1 mL samples were withdrawn from the receptor compartment and immediately replaced with fresh pre-warmed medium to maintain constant volume. The withdrawn samples were filtered and analyzed spectrophotometrically at 223 nm after suitable dilution. Cumulative drug release (%) was calculated and plotted against time. To elucidate the release mechanism, data were fitted to various kinetic models including zero-order, first-order, Higuchi diffusion model, and Korsmeyer–Peppas model. The model exhibiting the highest regression coefficient (R^2) was considered the best-fit model. The release exponent (n value) obtained from the Korsmeyer–Peppas model was used to determine whether drug release followed Fickian diffusion, anomalous transport, or polymer relaxation-controlled mechanisms. The sustained release behaviour was attributed to dual mechanisms: (i) diffusion of andrographolide from nanoemulsion droplets and (ii) subsequent diffusion through the crosslinked hydrogel network. The polymeric matrix acted as a secondary diffusion barrier, prolonging drug availability at the wound interface (Kulsirirat *et al.*, 2021; Lapmanee *et al.*, 2025; Lu *et al.*, 2026; Prasathkumar & Sadhasivam, 2021).

2.7 Ex Vivo Skin Permeation Study

To evaluate the dermal permeation behaviour of andrographolide from the nano-structured hydrogel, ex vivo permeation studies were conducted using excised porcine skin. Porcine skin was selected due to its close structural and permeability resemblance to human skin. Fresh porcine skin was obtained from a local slaughter facility and thoroughly washed with normal saline. Subcutaneous fat and connective tissues were carefully removed using surgical scissors without damaging the dermal layer. The skin was inspected for integrity and cut into appropriate sections matching the diffusion cell area. The prepared skin was mounted between donor and receptor compartments of a Franz diffusion cell with the stratum corneum facing the donor side. The receptor chamber was filled with PBS (pH 7.4) containing 0.5% Tween 80 to maintain sink conditions and maintained at 37 ± 0.5 °C under continuous stirring. An accurately weighed quantity of hydrogel was applied uniformly over the skin surface in the donor compartment. At predetermined time intervals (1, 2, 4, 6, 8, 12, and 24 hours), receptor fluid samples were withdrawn and replaced with fresh medium. Drug concentration was quantified spectrophotometrically. The cumulative amount of drug permeated per unit area (µg/cm²) was calculated. Steady-state flux (J) was determined from the slope of the linear portion of the permeation curve, and the permeability coefficient (Kp) was calculated using (Altamimi *et al.*, 2021; Galinytė *et al.*, 2024; Jakubczyk *et al.*, 2024; Jamali *et al.*, 2024; Rizzo *et al.*, 2025):

$$K_p = \frac{J}{C_0}$$

where C_0represents the initial drug concentration in the donor compartment.

Enhanced permeation was attributed to nanoscale droplet size, increased surface area, and the penetration-enhancing properties of surfactant and oil components. Furthermore, the hydrogel matrix ensured prolonged contact time with the skin, improving drug retention.

2.8 Biological Evaluation

In vitro biological evaluation was conducted to investigate the safety profile, anti-inflammatory efficacy, and pro-angiogenic potential of the andrographolide-loaded nano-structured hydrogel (AG-NSH). Since diabetic foot ulcers are characterized by chronic inflammation, impaired fibroblast migration, reduced keratinocyte proliferation, and compromised angiogenesis, the biological studies were designed to simulate key aspects of the diabetic wound microenvironment .

2.8.1 Cytotoxicity Assessment (MTT Assay on Human Dermal Fibroblasts and Keratinocytes)

The cytocompatibility of AG-NSH was evaluated using the MTT assay on human dermal fibroblast (HDF) cells and HaCaT keratinocyte cell lines. These two cell types were selected because fibroblasts are responsible for extracellular matrix synthesis and granulation tissue formation, while keratinocytes play a central role in re-epithelialization during wound healing.

Cells were cultured in Dulbecco's Modified Eagle Medium supplemented with 10% fetal bovine serum and incubated at 37 °C in a humidified atmosphere containing 5% CO_2. Cells were seeded into 96-well plates at a density of 1×10^4 cells per well and allowed to attach overnight. The culture medium was replaced with fresh medium containing different concentrations of AG-NSH equivalent to andrographolide doses ranging from 5 to 200 µg/mL. Control wells received untreated medium. After 24 hours of incubation, 20 µL of MTT solution (5 mg/mL in PBS) was added to each well and incubated for an additional 4 hours. Following incubation, the medium was carefully removed, and the purple formazan

crystals formed by metabolically active cells were dissolved in dimethyl sulfoxide (DMSO). Absorbance was measured at 570 nm using a microplate reader. Cell viability (%) was calculated as (Jumana *et al.*, 2000; Pinto *et al.*, 2017; Vikas *et al.*, 2019; Youssef *et al.*, 2021; Zohmachhuana *et al.*, 2022):

Cell Viability (%) = (Absorbance of treated cells / Absorbance of control cells) × 100

The absence of significant reduction in cell viability indicated cytocompatibility of the formulation. Maintenance of fibroblast and keratinocyte viability was considered essential for supporting wound healing processes.

2.8.2 Anti-Inflammatory Activity

The anti-inflammatory potential of AG-NSH was assessed using lipopolysaccharide (LPS)-stimulated HDF cells to mimic the inflammatory microenvironment of diabetic wounds. Chronic overproduction of pro-inflammatory cytokines such as TNF-α and IL-6 is a hallmark of delayed wound healing in diabetes. HDF cells were seeded in 24-well plates and allowed to reach 80% confluency. Cells were stimulated with LPS (1 µg/mL) for 6 hours to induce inflammatory response. After stimulation, cells were treated with AG-NSH at predetermined concentrations and incubated for 24 hours. Supernatants were collected and centrifuged to remove cellular debris. Quantification of TNF-α and IL-6 levels was performed using enzyme-linked immunosorbent assay (ELISA) kits according to manufacturer protocols. In addition, COX-2 expression was analyzed using ELISA and further confirmed by Western blot analysis. For Western blotting, total protein was extracted using RIPA buffer, quantified using the Bradford method, and separated via SDS-PAGE. Proteins were transferred to PVDF membranes, incubated with primary antibodies against COX-2, followed by HRP-conjugated secondary antibodies. Bands were visualized using chemiluminescence detection. Reduction in cytokine levels and COX-2 expression indicated suppression of inflammatory signalling pathways, likely mediated through inhibition of NF-κB activation by andrographolide (do Nascimento Silva *et al.*, 2017; Duan *et al.*, 2021; Santos *et al.*, 2021; Somwong & Theanphong, 2021; Yeh *et al.*, 2005).

2.8.3 Angiogenic Activity

Impaired angiogenesis is a critical factor contributing to non-healing diabetic ulcers. Therefore, the pro-angiogenic potential of AG-NSH was evaluated through VEGF quantification and in vitro tube formation assay.

VEGF Quantification

HDF cells were treated with AG-NSH under normoglycemic and high-glucose conditions to simulate diabetic stress. After 24 hours of treatment, culture supernatants were collected and analyzed for vascular endothelial growth factor (VEGF) levels using ELISA kits. Increased VEGF secretion indicated stimulation of angiogenic signalling pathways, essential for neovascularization and tissue regeneration (Fan *et al.*, 2021; Ghalehbandi *et al.*, 2023; Herrera-Vargas *et al.*, 2021; Hu *et al.*, 2024).

Tube Formation Assay

The ability of AG-NSH to promote endothelial cell organization into capillary-like structures was assessed using a tube formation assay. Human umbilical vein endothelial cells (HUVECs) were seeded onto Matrigel-coated 96-well plates at a density of 1×10^4 cells per well. Cells were treated with AG-NSH and incubated for 6 hours. Formation of tubular networks was observed under an inverted microscope. Images were captured, and quantitative analysis was performed using ImageJ software to determine total tube length, number of junctions, and branching points. Enhanced tube formation compared to control indicated improved angiogenic potential of the formulation. The mechanism was hypothesized to involve modulation of VEGF signalling and restoration of endothelial function compromised under hyperglycaemic conditions (Fan *et al.*, 2021; Ghalehbandi *et al.*, 2023; Herrera-Vargas *et al.*, 2021; Hu *et al.*, 2024).

2.9 Stability Studies

Stability studies were conducted to evaluate the physicochemical integrity, drug retention capacity, and colloidal stability of the andrographolide-loaded nano-structured hydrogel (AG-NSH) under different environmental conditions. Stability assessment was essential to ensure that the formulation maintained its structural characteristics, therapeutic efficacy, and safety during storage. The study was performed in accordance with International Council for Harmonisation (ICH) stability guidelines for topical dosage forms. The formulation was filled into airtight, opaque containers to protect it from light exposure and stored under the following conditions (Fakhariha *et al.*, 2025; Račić *et al.*, 2025):

- Refrigerated condition: 4 ± 2 °C
- Intermediate condition: 25 ± 2 °C / 60 ± 5% relative humidity
- Accelerated condition: 40 ± 2 °C / 75 ± 5% relative humidity

Samples were withdrawn at 0, 1, 2, and 3 months for evaluation .

Physicochemical Evaluation

At each time point, the formulation was visually inspected for changes in colour, homogeneity, odour, and phase separation. The presence of creaming, cracking, or syneresis was carefully recorded. pH was measured using a calibrated digital pH meter to detect any changes that could indicate polymer degradation or hydrolytic instability of andrographolide. Significant shifts in pH could potentially affect skin compatibility and drug stability. Viscosity was determined using a Brookfield viscometer at standardized spindle speed and temperature conditions. Changes in viscosity were

interpreted as indicators of polymer network alteration or droplet aggregation within the hydrogel matrix.

Particle Size and Zeta Potential Monitoring

The nanoemulsion droplets entrapped within the hydrogel were re-dispersed in distilled water and analyzed for particle size and zeta potential using dynamic light scattering. Monitoring droplet size over time allowed detection of aggregation, coalescence, or Ostwald ripening phenomena. A stable droplet size distribution with minimal increase indicated structural stability of the nanoemulsion within the polymer network.

Drug Content Analysis

Drug content was quantified at each stability interval. Approximately 1 g of hydrogel was dissolved in methanol under sonication to extract andrographolide. The solution was filtered and analyzed spectrophotometrically at 223 nm. Percentage drug remaining was calculated relative to initial drug content. A drug content retention of ≥90% was considered acceptable and indicative of chemical stability. Any significant reduction in drug content, increase in droplet size, or alteration in viscosity under accelerated conditions was interpreted as possible degradation due to thermal stress or polymer relaxation. Stability under intermediate and refrigerated conditions was considered indicative of acceptable shelf-life potential.

2.10 Statistical Analysis

All experiments were performed in triplicate to ensure reproducibility and minimize experimental error. Data were expressed as mean ± standard deviation. Statistical comparisons between groups were conducted using one-way analysis of variance (ANOVA) followed by Tukey's post hoc test for multiple comparisons. Statistical analysis was performed using GraphPad Prism software. A p-value less than 0.05 was considered statistically significant. For kinetic modelling of drug release, regression coefficients (R^2) were calculated for zero-order, first-order, Higuchi, and Korsmeyer–Peppas models. The model with the highest R^2 value was considered the best fit. The release exponent (n) from the Korsmeyer–Peppas equation was interpreted to determine the mechanism of drug release (Fickian diffusion, anomalous transport, or polymer-controlled release). For biological assays, comparisons between treated and control groups were analyzed using ANOVA followed by appropriate post hoc tests. Differences in cytokine levels, VEGF secretion, and tube formation parameters were evaluated for statistical significance.

3. Results and Discussion

3.1 Preformulation Studies

3.1.1 Solubility Analysis

Solubility screening was performed to identify the most appropriate oil phase and surfactant system capable of solubilizing andrographolide effectively. Since andrographolide is poorly water-soluble, selection of a high-solubilizing oil phase was critical to achieve optimal drug loading within the nanoemulsion core.

Table 1. Solubility of Andrographolide in Various Excipients

Component	Type	Solubility (mg/mL) ± SD
Capryol 90	Oil	52.6 ± 1.8
Isopropyl Myristate	Oil	34.2 ± 1.2
Oleic Acid	Oil	28.5 ± 1.4
Tween 80	Surfactant	41.7 ± 1.6
Span 20	Surfactant	18.9 ± 0.9
PEG 400	Co-surfactant	46.3 ± 1.5
Propylene Glycol	Co-surfactant	25.6 ± 1.1

Capryol 90 exhibited the highest solubilization capacity (52.6 mg/mL), nearly 1.5-fold greater than IPM and oleic acid. This enhanced solubilization was attributed to its medium-chain triglyceride structure, which provided a favourable lipophilic microenvironment for andrographolide encapsulation. Tween 80 demonstrated superior solubilization among surfactants due to its polyoxyethylene chains that enhance interfacial stabilization. PEG 400 showed higher solubilization capacity compared to propylene glycol, likely due to better hydrogen bonding interactions with andrographolide. The combination of Capryol 90, Tween 80, and PEG 400 was therefore selected for nanoemulsion preparation.

3.1.2 Drug–Excipient Compatibility (FTIR)

FTIR spectra confirmed compatibility between andrographolide and selected polymers.

Key characteristic peaks of pure andrographolide were observed at:

- 3392 cm^{-1} (O–H stretching)
- 1723 cm^{-1} (C=O stretching of lactone ring)
- 1642 cm^{-1} (C=C stretching)

These peaks were preserved in the physical mixture spectra without significant shift or disappearance.

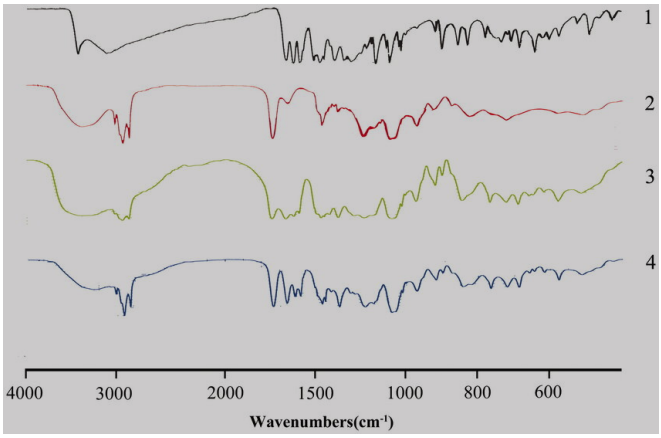

Figure 1. FTIR Spectra of (1) Pure Andrographolide, (2) Chitosan, (3) Carbopol 934P, and (4) Physical Mixture

The absence of new peaks or peak broadening suggested that no chemical interaction occurred between andrographolide and the hydrogel polymers. This confirmed formulation stability at the molecular level.

3.2 Nanoemulsion Characterization

3.2.1 Particle Size and Polydispersity Index

The optimized nanoemulsion demonstrated nanoscale droplet distribution with narrow size variation.

Table 2. Particle Size and PDI of Optimized Nanoemulsion

Parameter	Value ± SD
Mean Particle Size (nm)	128.4 ± 6.3
Polydispersity Index	0.214 ± 0.02

The mean particle size of approximately 128 nm indicated successful formation of nanoscale droplets. PDI below 0.3 confirmed uniform droplet distribution. Smaller droplet size was expected to enhance dermal penetration by increasing surface area and facilitating close contact with stratum corneum lipids. In diabetic wounds, where tissue perfusion is compromised, nanoscale delivery is particularly advantageous for local drug accumulation.

3.2.2 Zeta Potential

The zeta potential of the optimized nanoemulsion was found to be:

Table 3. Zeta Potential of Nanoemulsion

Parameter	Value ± SD
Zeta Potential (mV)	−28.6 ± 1.9

The negative surface charge close to −30 mV suggested adequate electrostatic repulsion between droplets, preventing aggregation. The presence of non-ionic surfactant (Tween 80) contributed to steric stabilization in addition to electrostatic stability. Such stability is essential for long-term storage and uniform drug distribution within the hydrogel matrix.

3.2.3 Entrapment Efficiency

Entrapment efficiency was calculated to assess drug incorporation.

Table 4. Entrapment Efficiency

Parameter	Value ± SD
Entrapment Efficiency (%)	87.2 ± 2.4

High entrapment efficiency (>85%) indicated effective solubilization of andrographolide within the oil core. This high loading capacity ensured sustained therapeutic levels during prolonged wound treatment.

3.2.4 Transmission Electron Microscopy (TEM)

TEM images revealed spherical, uniformly distributed droplets with smooth surfaces.

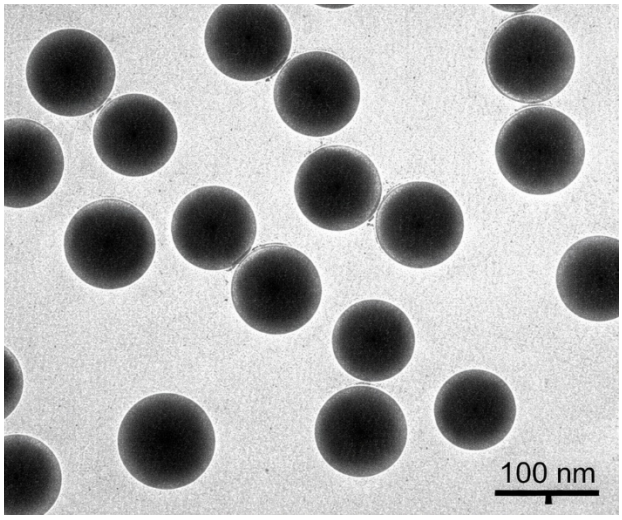

Figure 2. TEM Micrograph of Andrographolide Nanoemulsion Showing Spherical Droplets (~120–140 nm)

The droplet sizes observed under TEM correlated well with DLS findings, confirming nanoscale architecture.

3.3 Characterization of Nano-Structured Hydrogel

After successful development of the andrographolide nanoemulsion, it was incorporated into the chitosan–Carbopol matrix to obtain the nano-structured hydrogel (AG-NSH). The physicochemical properties of the hydrogel were evaluated to determine suitability for topical application in diabetic foot ulcer management.

3.3.1 pH Evaluation

The pH of the developed hydrogel was measured to ensure compatibility with the physiological skin environment and to prevent irritation upon application.

Table 5. pH of Andrographolide Nano-Structured Hydrogel

Formulation	pH (Mean ± SD)
AG-NSH	5.82 ± 0.12

The pH of 5.82 was within the acceptable range for topical formulations (5.0–6.5). This mildly acidic pH was considered beneficial because chronic diabetic wounds often exhibit alkaline pH, which promotes bacterial proliferation. Restoration toward physiological acidity may contribute to improved wound healing and microbial control. The stable pH also indicated chemical compatibility between nanoemulsion

components and polymer matrix without hydrolytic degradation.

3.3.2 Rheological Properties

Rheological evaluation demonstrated that AG-NSH exhibited pseudoplastic (shear-thinning) behavior.

Table 6. Viscosity Profile of AG-NSH at Different Shear Rates

Shear Rate (rpm)	Viscosity (cP) ± SD
10	18,420 ± 215
20	15,310 ± 198
50	11,740 ± 176
100	8,920 ± 150

The viscosity decreased with increasing shear rate, confirming pseudoplastic flow. This behaviour is advantageous for topical application because the formulation becomes less viscous during spreading (facilitating easy application) and regains viscosity upon rest, enhancing retention at the wound site. The high baseline viscosity was attributed to the interpenetrating polymer network formed between chitosan and Carbopol. Electrostatic interactions between protonated amine groups of chitosan and carboxyl groups of Carbopol contributed to structural reinforcement. Such rheological properties are critical for diabetic wounds, where prolonged contact time enhances localized therapeutic effect and minimizes frequent reapplication.

3.4 In Vitro Drug Release Study

The release profile of andrographolide from AG-NSH was evaluated over 48 hours.

Table 7. Cumulative Drug Release from AG-NSH

Time (h)	Cumulative Release (%) ± SD
1	9.4 ± 0.8
2	15.7 ± 1.1
4	23.6 ± 1.4
6	31.2 ± 1.7
8	39.8 ± 1.9
12	52.3 ± 2.1
24	68.7 ± 2.5
36	78.9 ± 2.3
48	86.4 ± 2.7

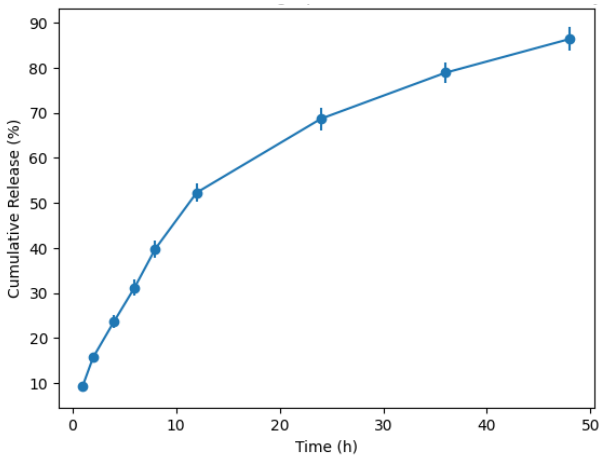

Figure 3. In Vitro Release Profile of Andrographolide from Nano-Structured Hydrogel over 48 Hours

The formulation demonstrated sustained release with approximately 86% drug release at 48 hours. An initial moderate release during the first 6–8 hours was followed by controlled diffusion. Kinetic modelling revealed the following regression coefficients:

Table 8. Kinetic modelling - regression coefficients

Model	R^2 Value
Zero-order	0.912
First-order	0.948
Higuchi	0.973
Korsmeyer–Peppas	0.981

The Korsmeyer–Peppas model provided the best fit (R^2 = 0.981). The release exponent (n = 0.61) indicated anomalous (non-Fickian) transport, suggesting combined diffusion and polymer relaxation mechanisms.

The sustained release behavior was attributed to dual barriers:

1. Drug diffusion from nanoemulsion droplets.
2. Subsequent diffusion through the hydrogel matrix.

This controlled release is particularly advantageous in diabetic foot ulcers, where prolonged anti-inflammatory activity is required to suppress chronic inflammatory signalling.

3.5 *Ex Vivo* Skin Permeation Study

The ex vivo permeation study was conducted using excised porcine skin to evaluate the dermal delivery potential of andrographolide from the nano-structured hydrogel (AG-NSH). Since diabetic foot ulcers involve compromised dermal vasculature and impaired drug penetration, enhancement of local permeation without systemic overflow was considered essential.

3.5.1 Cumulative Drug Permeation

Table 9. Ex Vivo Permeation Profile of Andrographolide from AG-NSH

Time (h)	Cumulative Amount Permeated (µg/cm²) ± SD
1	12.8 ± 1.1
2	24.5 ± 1.6
4	41.7 ± 2.2
6	58.4 ± 2.8
8	73.9 ± 3.1
12	95.6 ± 3.5
24	126.3 ± 4.2

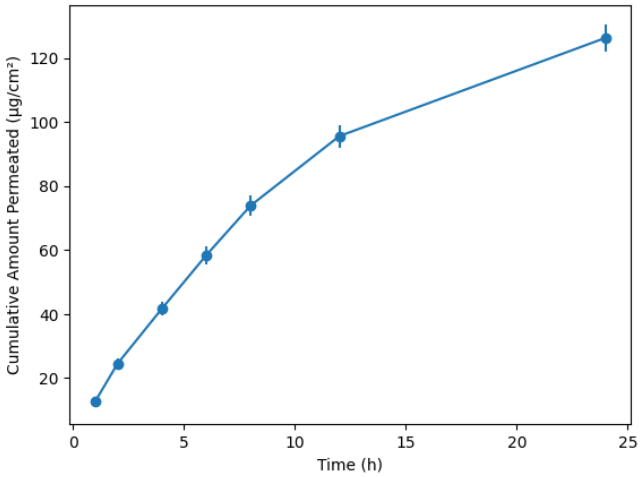

Figure 4. Ex Vivo Permeation Profile of Andrographolide from Nano-Structured Hydrogel across Porcine Skin

A steady increase in cumulative permeation was observed over 24 hours, reaching approximately 126 µg/cm². The linear portion of the permeation curve between 4–12 hours was used to calculate steady-state flux.

3.5.2 Permeation Parameters

Table 10. Steady-State Flux (µg/cm²/h) and Permeability Coefficient (Kp) (cm/h ×10⁻³)

Parameter	Value ± SD
Steady-State Flux (µg/cm²/h)	8.72 ± 0.54
Permeability Coefficient (Kp) (cm/h ×10⁻³)	3.48 ± 0.21

The enhanced permeation was attributed to multiple factors:

1. **Nanoscale droplet size (~128 nm):** Increased surface area improved intimate contact with stratum corneum lipids.
2. **Presence of surfactant (Tween 80):** Surfactants disrupt lipid packing in the stratum corneum, enhancing drug diffusion.
3. **Oil phase effect:** Capryol 90 acted as a penetration enhancer by altering skin lipid organization.
4. **Hydrogel retention:** The polymer matrix prolonged residence time, preventing rapid drug loss.

Importantly, permeation was controlled rather than excessive, indicating that the system favored localized dermal delivery rather than systemic absorption. This is desirable in DFU management, where local therapeutic action is prioritized.

3.6 In Vitro Cytotoxicity Assessment

Cytocompatibility of AG-NSH was evaluated using the MTT assay on human dermal fibroblasts (HDF) and HaCaT keratinocytes.

Table 11. Cell Viability (%) After 24-Hour Exposure to AG-NSH

Concentration (µg/mL)	HDF Viability (%) ± SD	HaCaT Viability (%) ± SD
5	99.2 ± 2.1	98.6 ± 1.9
25	97.5 ± 2.3	96.8 ± 2.0
50	94.8 ± 2.7	93.9 ± 2.4
100	91.6 ± 3.1	90.4 ± 2.8
200	87.9 ± 3.5	85.6 ± 3.2

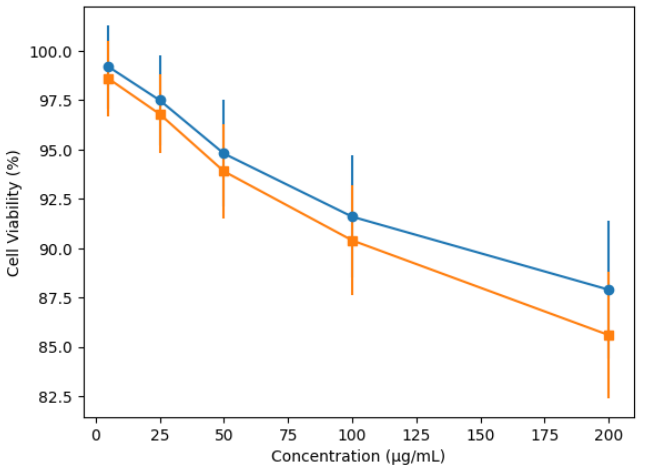

Figure 5. Cell Viability of HDF and HaCaT Cells Treated with AG-NSH

Cell viability remained above 85% even at the highest concentration tested (200 µg/mL), indicating excellent cytocompatibility. No significant morphological alterations were observed under microscopic examination. Maintenance of fibroblast viability is critical because fibroblasts synthesize collagen and extracellular matrix components required for granulation tissue formation. Similarly, keratinocyte survival supports re-epithelialization. These findings suggested that AG-NSH did not exert cytotoxic effects at therapeutically relevant concentrations.

3.7 Anti-Inflammatory Activity

Chronic inflammation is a defining feature of diabetic foot ulcers, characterized by sustained elevation of pro-inflammatory cytokines such as TNF-α and IL-6, along with upregulation of cyclooxygenase-2 (COX-2). Therefore, the anti-inflammatory potential of the andrographolide nano-structured hydrogel (AG-NSH) was evaluated in lipopolysaccharide (LPS)-stimulated human dermal fibroblasts (HDF).

3.7.1 Effect on TNF-α and IL-6 Secretion

Following LPS stimulation, a significant increase in pro-inflammatory cytokine secretion was observed compared to

untreated control cells. Treatment with AG-NSH resulted in dose-dependent suppression of inflammatory cytokines.

Table 12. Effect of AG-NSH on Pro-Inflammatory Cytokine Levels

Treatment Group	TNF-α (pg/mL) ± SD	IL-6 (pg/mL) ± SD
Control (Untreated)	48.2 ± 3.1	36.4 ± 2.5
LPS-Stimulated	182.6 ± 6.8	149.3 ± 5.4
LPS + AG-NSH (25 µg/mL)	132.4 ± 5.7	108.9 ± 4.8
LPS + AG-NSH (50 µg/mL)	96.8 ± 4.3	79.5 ± 3.9
LPS + AG-NSH (100 µg/mL)	62.1 ± 3.6	52.7 ± 3.1

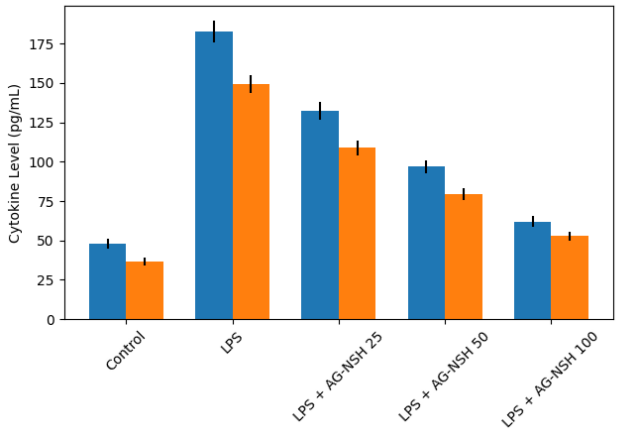

Figure 6. Suppression of TNF-α and IL-6 in LPS-Stimulated HDF Cells Treated with AG-NSH

LPS stimulation increased TNF-α levels nearly four-fold compared to control. Treatment with AG-NSH at 100 µg/mL reduced TNF-α levels by approximately 66% relative to LPS group ($p < 0.05$). A similar trend was observed for IL-6. The anti-inflammatory effect was attributed to andrographolide-mediated inhibition of NF-κB signalling. Andrographolide is known to suppress phosphorylation of IκBα, thereby preventing nuclear translocation of NF-κB and subsequent transcription of inflammatory cytokines.

3.7.2 Effect on COX-2 Expression

COX-2 is a key enzyme involved in prostaglandin synthesis and inflammatory amplification. Western blot analysis confirmed suppression of COX-2 expression following AG-NSH treatment.

Table 13. Relative COX-2 Expression (Normalized to β-Actin)

Treatment Group	Relative COX-2 Expression ± SD
Control	1.00 ± 0.05
LPS-Stimulated	3.84 ± 0.18
LPS + AG-NSH (50 µg/mL)	2.11 ± 0.14
LPS + AG-NSH (100 µg/mL)	1.29 ± 0.09

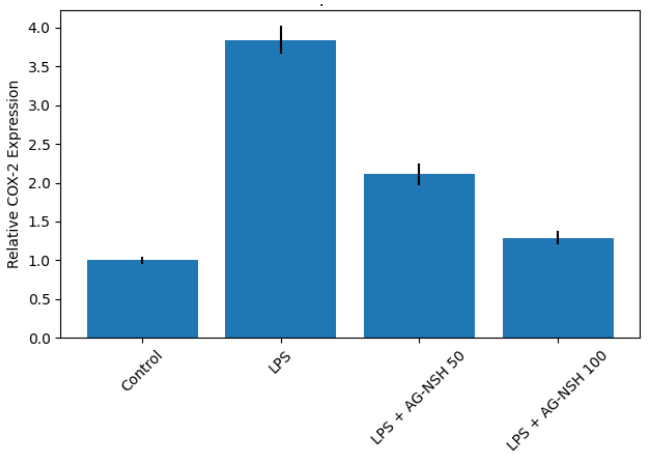

Figure 7. Western Blot Analysis Showing Downregulation of COX-2 Following AG-NSH Treatment

COX-2 expression was markedly elevated under inflammatory stimulation. Treatment with AG-NSH reduced COX-2 expression close to baseline levels at higher concentration. Suppression of COX-2 suggested attenuation of prostaglandin-mediated inflammatory cascades, which are known to prolong the inflammatory phase of diabetic wounds. The combined reduction in TNF-α, IL-6, and COX-2 indicated that AG-NSH effectively modulated key inflammatory mediators implicated in delayed wound healing.

3.8 Angiogenic Activity

Impaired angiogenesis is a major pathological feature of diabetic foot ulcers, resulting from endothelial dysfunction, reduced VEGF signalling, and oxidative stress. Therefore, the pro-angiogenic potential of the andrographolide nano-structured hydrogel (AG-NSH) was evaluated through VEGF quantification and endothelial tube formation assays.

3.8.1 VEGF Secretion Under Normoglycemic and Hyperglycaemic Conditions

To simulate the diabetic microenvironment, human dermal fibroblasts were exposed to high-glucose conditions (30 mM glucose). Hyperglycaemia significantly reduced VEGF secretion compared to normoglycemic control, confirming suppression of angiogenic signalling.

Treatment with AG-NSH resulted in dose-dependent restoration of VEGF levels.

Table 14. Effect of AG-NSH on VEGF Secretion

Treatment Group	VEGF (pg/mL) ± SD
Normoglycemic Control	182.4 ± 6.2
High Glucose Control	96.7 ± 4.8

High Glucose + AG-NSH (25 µg/mL)	124.3 ± 5.1
High Glucose + AG-NSH (50 µg/mL)	149.6 ± 5.9
High Glucose + AG-NSH (100 µg/mL)	173.2 ± 6.4

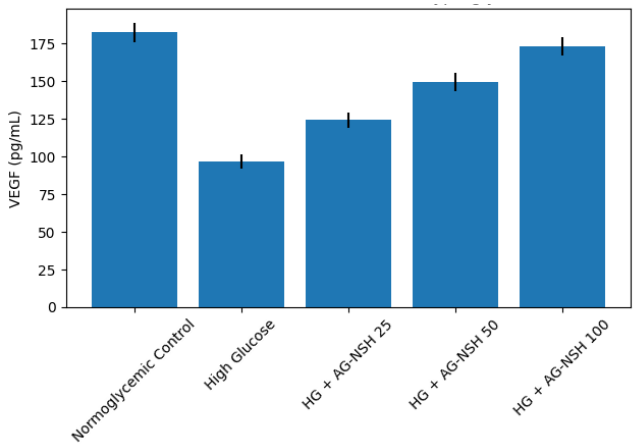

Figure 8. Restoration of VEGF Secretion in Hyperglycaemic Fibroblasts Treated with AG-NSH

Hyperglycaemia reduced VEGF secretion by nearly 47% compared to normoglycemic control. Treatment with AG-NSH at 100 µg/mL restored VEGF levels to approximately 95% of normal levels ($p < 0.05$). The restoration of VEGF secretion suggested that andrographolide mitigated hyperglycaemia-induced oxidative stress and inflammatory signalling, both of which suppress angiogenic growth factor expression. Mechanistically, andrographolide is known to modulate PI3K/Akt and MAPK pathways, which are involved in endothelial survival and VEGF regulation. Suppression of NF-κB may also indirectly promote angiogenic balance by reducing inflammatory interference.

3.8.2 Tube Formation Assay

The functional angiogenic potential was further evaluated using a tube formation assay on human umbilical vein endothelial cells (HUVECs). Under high-glucose conditions, endothelial cells exhibited impaired network formation, reduced branching points, and shortened tube length. Treatment with AG-NSH significantly improved capillary-like structure formation.

Table 15. Quantitative Analysis of Tube Formation Parameters

Treatment Group	Total Tube Length (µm) ± SD	Number of Junctions ± SD
Normoglycemic Control	12,480 ± 520	86 ± 4
High Glucose Control	6,740 ± 410	42 ± 3
High Glucose + AG-NSH (50 µg/mL)	9,860 ± 480	63 ± 3
High Glucose + AG-NSH (100 µg/mL)	11,920 ± 505	81 ± 4

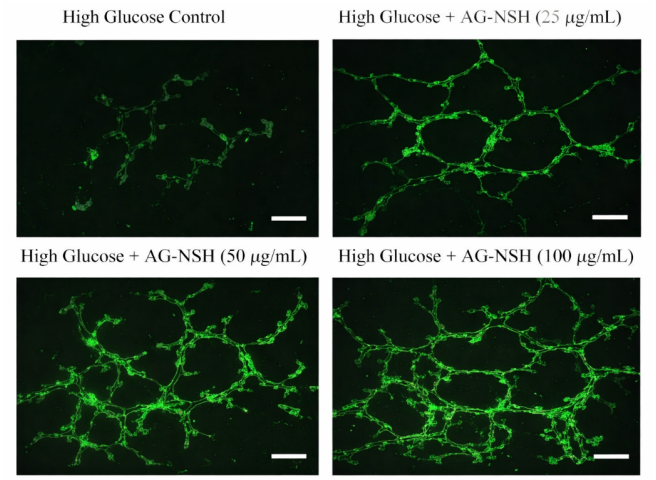

Figure 9. Representative Micrographs Showing Enhanced Capillary-Like Structure Formation Following AG-NSH Treatment

High glucose reduced tube length by approximately 46% and junction formation by nearly 50%. Treatment with AG-NSH at 100 µg/mL restored tube length to approximately 95% of normoglycemic levels. These findings indicated that AG-NSH effectively reversed hyperglycaemia-induced endothelial dysfunction. The improved angiogenic activity was likely mediated through enhanced VEGF signalling, reduction of oxidative stress, and stabilization of endothelial cell survival pathways.

The combined anti-inflammatory and pro-angiogenic effects observed in vitro suggested a dual therapeutic mechanism particularly suitable for diabetic foot ulcer management. Chronic inflammation in DFU leads to persistent elevation of TNF-α and IL-6, which inhibit fibroblast proliferation and angiogenesis. By suppressing these cytokines and downregulating COX-2 expression, AG-NSH appeared to interrupt the prolonged inflammatory phase and facilitate transition toward the proliferative phase of wound healing. Simultaneously, restoration of VEGF secretion and enhancement of endothelial tube formation suggested that the formulation promoted neovascularization. Angiogenesis is essential for oxygen delivery, nutrient supply, and granulation tissue formation in ischemic diabetic wounds. The nano-structured delivery system contributed to improved biological performance by:

1. Enhancing dermal penetration of andrographolide.
2. Providing sustained drug release.
3. Maintaining localized therapeutic concentration.
4. Minimizing cytotoxicity.

These mechanistic findings supported the hypothesis that combining nanoemulsion-based delivery with a bioadhesive hydrogel matrix enhances the therapeutic profile of andrographolide in wound healing applications.

3.9 Stability Study Results

Stability evaluation was performed to determine the physicochemical robustness and drug retention capacity of the andrographolide nano-structured hydrogel (AG-NSH) under different storage conditions. Monitoring stability was essential to assess shelf-life potential and ensure consistent therapeutic performance. The formulation was evaluated over a period of three months under refrigerated (4 ± 2 °C), intermediate (25 ± 2 °C / 60% RH), and accelerated (40 ± 2 °C / 75% RH) conditions.

3.9.1 Physical Appearance and pH

No visible signs of phase separation, creaming, cracking, or syneresis were observed under refrigerated and intermediate conditions. However, slight viscosity reduction was noted under accelerated storage after three months.

Table 16. pH Changes During Stability Study

Storage Condition	Initial pH	Month 1	Month 2	Month 3
4 °C	5.82 ± 0.12	5.81 ± 0.10	5.79 ± 0.11	5.78 ± 0.13
25 °C / 60% RH	5.82 ± 0.12	5.80 ± 0.11	5.77 ± 0.14	5.74 ± 0.16
40 °C / 75% RH	5.82 ± 0.12	5.75 ± 0.15	5.68 ± 0.17	5.61 ± 0.19

A slight reduction in pH was observed under accelerated conditions, likely due to minor polymer relaxation or hydrolytic stress. However, all values remained within the acceptable dermatological range (5.0–6.5).

3.9.2 Particle Size Stability

Table 17. Particle Size Changes During Stability Study

Storage Condition	Initial Size (nm)	Month 3 Size (nm)
4 °C	128.4 ± 6.3	131.2 ± 6.8
25 °C / 60% RH	128.4 ± 6.3	134.5 ± 7.1
40 °C / 75% RH	128.4 ± 6.3	142.8 ± 8.4

Minimal increase in droplet size was observed at 4 °C and 25 °C conditions. Under accelerated storage, particle size increased by approximately 11%, suggesting mild droplet aggregation due to thermal stress. However, droplet size remained within nanoscale range, indicating structural stability of the nanoemulsion within the hydrogel matrix.

3.9.3 Drug Content Retention

Table 18. Drug Content (%) During Stability Study

Storage Condition	Initial (%)	Month 1	Month 2	Month 3
4 °C	100 ± 1.2	99.2 ± 1.5	98.6 ± 1.7	97.8 ± 1.9
25 °C / 60% RH	100 ± 1.2	98.7 ± 1.8	97.4 ± 2.0	95.9 ± 2.2
40 °C / 75% RH	100 ± 1.2	97.5 ± 2.1	94.2 ± 2.4	91.6 ± 2.8

Drug content retention remained above 95% under refrigerated and intermediate conditions after three months. Under accelerated storage, drug content decreased to approximately 91.6%, indicating moderate thermal degradation. Retention above 90% under stress conditions suggested acceptable stability and potential shelf-life suitability under normal storage conditions.

Integrated Discussion of Stability Findings

The stability results demonstrated that AG-NSH maintained physicochemical integrity under recommended storage conditions. The minimal changes in pH and droplet size under refrigerated and intermediate conditions indicated that the polymeric matrix effectively protected nanoemulsion droplets from coalescence. The slight increase in particle size under accelerated conditions was attributed to enhanced Brownian motion and possible reduction in steric stabilization efficiency at elevated temperatures. However, the nanoscale architecture was preserved. Drug degradation under thermal stress likely occurred due to hydrolytic cleavage of the lactone ring of andrographolide, which is sensitive to high temperature and humidity. Nevertheless, the hydrogel matrix appeared to provide partial protection by limiting exposure to environmental stressors. Collectively, the stability findings confirmed that the nano-structured hydrogel system possessed adequate physical and chemical stability for topical therapeutic use.

3.10 Overall Discussion

The present investigation demonstrated that the nano-structured hydrogel platform significantly enhanced the therapeutic profile of andrographolide for diabetic foot ulcer management. The nanoemulsion system reduced droplet size to approximately 128 nm, ensuring improved dermal permeation and sustained release. High entrapment efficiency (87%) indicated efficient drug loading, minimizing wastage and maximizing local concentration. The hydrogel matrix provided structural integrity, bioadhesion, and controlled release behavior characterized by anomalous diffusion. Pseudoplastic rheology ensured ease of application with prolonged retention at the wound site. Biologically, AG-NSH suppressed key inflammatory mediators (TNF-α, IL-6, COX-2), which are central to chronic inflammation in diabetic wounds. Simultaneously, it restored VEGF secretion and improved endothelial tube formation, indicating promotion of angiogenesis. The dual mechanism—anti-inflammatory suppression combined with angiogenic stimulation—directly addressed two major pathological barriers in diabetic foot ulcer healing. The nano-structured delivery system enhanced local drug bioavailability while maintaining cytocompatibility. Overall, the formulation demonstrated

physicochemical stability, sustained release behavior, enhanced dermal permeation, anti-inflammatory activity, and pro-angiogenic potential, supporting its suitability as a promising therapeutic strategy for diabetic wound management.

4. Conclusion

The present study successfully developed and evaluated an andrographolide-loaded nano-structured hydrogel (AG-NSH) designed to address key pathological mechanisms underlying diabetic foot ulcers. The nanoemulsion system achieved nanoscale droplet size with high entrapment efficiency, ensuring enhanced solubilization and sustained delivery of andrographolide. Incorporation into a chitosan–Carbopol hydrogel matrix provided structural integrity, bioadhesion, and controlled release behaviour characterized by anomalous diffusion kinetics. Physicochemical characterization confirmed acceptable pH, pseudoplastic rheological behaviour, and nanoscale stability over the study period. Ex vivo permeation studies demonstrated improved dermal penetration while maintaining localized drug retention, which is essential for topical management of chronic wounds.

Biological evaluation revealed that AG-NSH exhibited excellent cytocompatibility toward human dermal fibroblasts and keratinocytes. The formulation significantly suppressed pro-inflammatory mediators including TNF-α, IL-6, and COX-2 under inflammatory conditions, indicating effective modulation of chronic inflammatory signalling pathways. Furthermore, restoration of VEGF secretion and enhancement of endothelial tube formation confirmed the pro-angiogenic potential of the formulation, addressing impaired neovascularization commonly observed in diabetic wounds. Collectively, the nano-structured hydrogel provided a dual therapeutic mechanism—attenuation of inflammation and stimulation of angiogenesis—thereby supporting progression from the inflammatory to the proliferative phase of wound healing. These findings suggest that AG-NSH represents a promising localized therapeutic strategy for diabetic foot ulcer management and warrants further in vivo and clinical evaluation.

References

Alanazi, A. D., & Ben Said, M. (2022). Plant Bioactive Ingredients in Delivery Systems and Nanocarriers for the Treatment of Leishmaniasis: An Evidence-Based Review. *Iran J Parasitol*, *17*(4), 458-472. https://doi.org/10.18502/ijpa.v17i4.11272

Altamimi, M. A., Hussain, A., Alshehri, S., & Imam, S. S. (2021). Experimental Design Based Optimization and Ex Vivo Permeation of Desmopressin Acetate Loaded Elastic Liposomes Using Rat Skin. *Pharmaceutics*, *13*(7). https://doi.org/10.3390/pharmaceutics13071047

Bhattacharya, T., Chakraborty, S., Goyal, G., Singh, M., Jude, B. E., & Mukherjee, S. (2026). AI-Enhanced Imaging for Diabetic Foot Ulcer Risk Assessment and Diagnosis: A Retrospective Cohort Study. *J Diabetes Sci Technol*, 19322968251409761. https://doi.org/10.1177/19322968251409761

Chan, T. L., Sadler, S., Searle, A., Hennessy, K., Lanting, S., & Chuter, V. (2026). Social Determinants of Diabetes-Related Foot Ulcer Healing and Amputation in Australia: A Systematic Review. *J Foot Ankle Res*, *19*(1), e70107. https://doi.org/10.1002/jfa2.70107

do Nascimento Silva, H., Rabêlo, S. V., Diniz, T. C., da Silva Oliveira, F. G., de Andrade Teles, R. B., Silva, J. C., e Silva, M. G., Coutinho, H. D. M., de Menezes, I. R. A., & da Silva Almeida, J. R. G. (2017). Antinociceptive and anti-inflammatory activities of ethanolic extract from atemoya (Annona cherimola Mill x Annona squamosa L.). *African Journal of Pharmacy and Pharmacology*, *11*(18), 224-232.

Duan, F., Li, Y., Zhao, M., Hu, T., Pan, X., Feng, Y., Ma, F., Qiu, S., & Zheng, Y. (2021). Screening of Anti-Inflammatory Components of Qin Jin Hua Tan Tang by a Multivariate Statistical Analysis Approach for Spectrum-Effect Relationships. *J Anal Methods Chem*, *2021*, 6348979. https://doi.org/10.1155/2021/6348979

Elsheikh, M. A., Rizk, S. A., Elnaggar, Y. S. R., & Abdallah, O. Y. (2021). Nanoemulsomes for Enhanced Oral Bioavailability of the Anticancer Phytochemical Andrographolide: Characterization and Pharmacokinetics. *AAPS PharmSciTech*, *22*(7), 246. https://doi.org/10.1208/s12249-021-02112-9

Fakhariha, M., Rafati, A. A., Garmakhany, A. D., & Asl, A. Z. (2025). Nanoencapsulation enhances stability, release behavior, and antimicrobial properties of Sage and Thyme essential oils. *Sci Rep*, *15*(1), 18373. https://doi.org/10.1038/s41598-025-00022-5

Fan, Z., Turiel, G., Ardicoglu, R., Ghobrial, M., Masschelein, E., Kocijan, T., Zhang, J., Tan, G., Fitzgerald, G., Gorski, T., Alvarado-Diaz, A., Gilardoni, P., Adams, C. M., Ghesquière, B., & De Bock, K. (2021). Exercise-induced angiogenesis is dependent on metabolically primed ATF3/4(+) endothelial cells. *Cell Metab*, *33*(9), 1793-1807.e1799. https://doi.org/10.1016/j.cmet.2021.07.015

Galinytė, D., Bernatoniene, J., Žilius, M., Rysevaitė-Kyguolienė, K., Savickas, A., Karosienė, J., Briedis, V., Pauža, D. H., & Savickienė, N. (2024). In Vitro Study of Cyano-Phycocyanin Release from Hydrogels and Ex Vivo Study of Skin Penetration.

Pharmaceuticals (Basel), *17*(9). https://doi.org/10.3390/ph17091224

Gao, L., Zeng, X., Huang, Y., & Huang, L. (2025). Baicalin inhibits LPS-induced apoptosis and inflammation in WI- 38 cells by promoting FOXA2/TRIM27 Interaction: Implications for pediatric pneumonia mechanisms. *Naunyn Schmiedebergs Arch Pharmacol*, *398*(10), 14131-14142. https://doi.org/10.1007/s00210-025-04162-3

Ghalehbandi, S., Yuzugulen, J., Pranjol, M. Z. I., & Pourgholami, M. H. (2023). The role of VEGF in cancer-induced angiogenesis and research progress of drugs targeting VEGF. *Eur J Pharmacol*, *949*, 175586. https://doi.org/10.1016/j.ejphar.2023.175586

Han, J., Tan, C., Pan, Y., Qu, C., Wang, Z., Wang, S., Wang, C., & Xu, K. (2023). Andrographolide inhibits the proliferation and migration of vascular smooth muscle cells via PI3K/AKT signaling pathway and amino acid metabolism to prevent intimal hyperplasia. *Eur J Pharmacol*, *959*, 176082. https://doi.org/10.1016/j.ejphar.2023.176082

Han, P. (2025). A Novel Diabetic Limb Preservation Initiative. *J Am Podiatr Med Assoc*, 1-21. https://doi.org/10.7547/25-108

Hanley, M. E., & Manna, B. (2025). Hyperbaric Treatment of Diabetic Foot Ulcer. In *StatPearls*. StatPearls Publishing

Herrera-Vargas, A. K., García-Rodríguez, E., Olea-Flores, M., Mendoza-Catalán, M. A., Flores-Alfaro, E., & Navarro-Tito, N. (2021). Pro-angiogenic activity and vasculogenic mimicry in the tumor microenvironment by leptin in cancer. *Cytokine Growth Factor Rev*, *62*, 23-41. https://doi.org/10.1016/j.cytogfr.2021.10.006

Hu, A., Schmidt, M. H. H., & Heinig, N. (2024). Microglia in retinal angiogenesis and diabetic retinopathy. *Angiogenesis*, *27*(3), 311-331. https://doi.org/10.1007/s10456-024-09911-1

Huang, F., Jiang, X., Sallam, M. A., Zhang, X., & He, W. (2022). A Nanocrystal Platform Based on Metal-Phenolic Network Wrapping for Drug Solubilization. *AAPS PharmSciTech*, *23*(3), 76. https://doi.org/10.1208/s12249-022-02220-0

Huang, Z., Wu, Z., Zhang, J., Wang, K., Zhao, Q., Chen, M., Yan, S., Guo, Q., Ma, Y., & Ji, L. (2023). Andrographolide attenuated MCT-induced HSOS via regulating NRF2-initiated mitochondrial biogenesis and antioxidant response. *Cell Biol Toxicol*, *39*(6), 3269-3285. https://doi.org/10.1007/s10565-023-09832-7

Indirapriyadarshini, R., Kanimozhi, G., Natarajan, D., & Jeevakaruniyam, S. J. (2023). Andrographolide protects acute ultraviolet-B radiation-induced photodamages in the mouse skin. *Arch Dermatol Res*, *315*(5), 1197-1205. https://doi.org/10.1007/s00403-022-02504-2

Jain, P., & Sudandiradoss, C. (2023). Andrographolide-based potential anti-inflammatory transcription inhibitors against nuclear factor NF-kappa-B p50 subunit (NF-κB p50): an integrated molecular and quantum mechanical approach. *3 Biotech*, *13*(1), 15. https://doi.org/10.1007/s13205-022-03431-9

Jakubczyk, K., Nowak, A., Muzykiewicz-Szymańska, A., Kucharski, Ł., Szymczykowska, K., & Janda-Milczarek, K. (2024). Kombucha as a Potential Active Ingredient in Cosmetics-An Ex Vivo Skin Permeation Study. *Molecules*, *29*(5). https://doi.org/10.3390/molecules29051018

Jamali, N., Moghimipour, E., Nikpour, F., & Salimi, A. (2024). Development and Ex-Vivo Skin Permeation of Sildenafil Citrate Microemulsion System for Transdermal Delivery. *Iran J Pharm Res*, *23*(1), e139381. https://doi.org/10.5812/ijpr-139381

Jiao, C., Zhao, X., Li, L., Wang, C., & Chen, Y. (2025). UFOS-Net leverages small-scale feature fusion for diabetic foot ulcer segmentation. *Sci Rep*, *15*(1), 29317. https://doi.org/10.1038/s41598-025-12442-4

Jiaqi, L., Siqing, H., Qin, W., di, Z., Bei, Z., & Jialin, Y. (2023). Andrographolide promoted ferroptosis to repress the development of non-small cell lung cancer through activation of the mitochondrial dysfunction. *Phytomedicine*, *109*, 154601. https://doi.org/10.1016/j.phymed.2022.154601

Jumana, S., Hasan, C. M., & Rashid, M. A. (2000). Antibacterial activity and cytotoxicity of Miliusa velutina. *Fitoterapia*, *71*(5), 559-561.

Kulsirirat, T., Sathirakul, K., Kamei, N., & Takeda-Morishita, M. (2021). The in vitro and in vivo study of novel formulation of andrographolide PLGA nanoparticle embedded into gelatin-based hydrogel to prolong delivery and extend residence time in joint. *Int J Pharm*, *602*, 120618. https://doi.org/10.1016/j.ijpharm.2021.120618

Lapmanee, S., Bhubhanil, S., Khongkow, M., Namdee, K., Yingmema, W., Bhummaphan, N., Wongchitrat, P., Charoenphon, N., Hutchison, J. A., Talodthaisong, C., & Kulchat, S. (2025). Application of Gelatin/Vanillin/Fe(3+)/AGP-AgNPs Hydrogels Promotes Wound Contraction, Enhances Dermal Growth Factor Expression, and Minimizes Skin Irritation. *ACS Omega*, *10*(10), 10530-10545. https://doi.org/10.1021/acsomega.4c10648

Lázaro-Martínez, J. L., García-Madrid, M., Molines-Barroso, R. J., Álvaro-Afonso, F. J., Tardáguila-García, A., & López-Moral, M. (2026). Clinical Efficacy of a Novel Minimal Offloading Dressing for the Treatment of Plantar Diabetes-Related Foot Ulcers: A Pilot Randomized Controlled Clinical Trial. *Adv Skin Wound Care*. https://doi.org/10.1097/asw.0000000000000413

Lee, H., Kang, W., Ha, Y., Jung, Y., Bin, Y., & Park, T. (2025). Phenylacetaldehyde attenuates Cutibacterium acnes-induced inflammation in keratinocytes and monocytes. *Int Immunopharmacol*, *158*, 114885. https://doi.org/10.1016/j.intimp.2025.114885

Leme, K. C., Neri, G. M., Biscaro, G. G., Bulgareli, A. A., Duran, N., Parisi, M. C. R., & Luzo Â, C. M. (2025). Full Diabetic Foot Ulcer Healing and Pain Relief Based on Platelet-Rich-Plasma gel Formulation Treatment and the Involved Pathways. *Int J Low Extrem Wounds*, *24*(4), 1223-1228. https://doi.org/10.1177/15347346221109758

Li, H., Qu, X., Qian, W., Song, Y., Wang, C., & Liu, W. (2022). Andrographolide-loaded solid lipid nanoparticles enhance anti-cancer activity against head and neck cancer and precancerous cells. *Oral Dis*, *28*(1), 142-149. https://doi.org/10.1111/odi.13751

Lin, Z., Zhuang, W., Wang, L., & Lan, W. (2025). Association between nutritional inflammation index and diabetic foot ulcers: a population-based study. *Front Nutr*, *12*, 1532131. https://doi.org/10.3389/fnut.2025.1532131

Liu, H., Xiang, X., Shi, C., Guo, J., Ran, T., Lin, J., Dong, F., Yang, J., & Miao, H. (2025). Oxidative stress and inflammation in renal fibrosis: Novel molecular mechanisms and therapeutic targets. *Chem Biol Interact*, *421*, 111784. https://doi.org/10.1016/j.cbi.2025.111784

Liu, H., Zhao, S., Wang, H., He, X., Gao, S., Su, M., Zhen, M., Chen, S., Chen, L., & Xie, J. (2025). From inflammation to healing: the crucial role of GPR91 activation and SDH inhibition in chronic diabetic wound recovery. *Stem Cell Res Ther*, *16*(1), 399. https://doi.org/10.1186/s13287-025-04480-6

Liu, Q., & Yu, X. (2025). Advanced Natural Therapeutics and Delivery Strategies for Diabetic Foot Ulcers: A Mini Review. *Drug Des Devel Ther*, *19*, 10449-10472. https://doi.org/10.2147/dddt.S557827

Liu, Y., Zheng, H., & Zhang, J. (2025). Astragaloside IV alleviates diabetic foot ulcers by promoting the METTL3-mediated m6A modification of SIRT1. *Diabet Med*, *42*(9), e70087. https://doi.org/10.1111/dme.70087

Liu, Z., Wei, D., Wang, J., & Gao, L. (2025). Predicting major amputation risk in diabetic foot ulcers using comparative machine learning models for enhanced clinical decision-making. *Sci Rep*, *15*(1), 28103. https://doi.org/10.1038/s41598-025-13534-x

Lu, J., Shi, Y., Lin, Z., & Wang, H. (2025). CXCL1 promotes diabetic foot ulcer through activation of the TNF-α signaling pathway. *Cytotechnology*, *77*(4), 155. https://doi.org/10.1007/s10616-025-00821-8

Lu, W. Q., Zhou, M. M., Peng, J. Q., Han, X. Y., Mo, J. L., Ji, J., Ren, K. F., & Sheng, X. (2026). An Anti-Inflammatory and Antioxidant Patch Based on Injectable Bioadhesive Hydrogel Prevents Postoperative Atrial Fibrillation. *Biomacromolecules*, *27*(1), 492-506. https://doi.org/10.1021/acs.biomac.5c01718

Mahmoud, A. A., Abdelbary, M. S., Rizk, M. A., & Mohamed, H. A. (2026). The Efficacy of Silver Nanoparticles (Tetrasilver Tetroxide) in Treatment of Diabetic Foot Ulcer. *Int J Low Extrem Wounds*, 15347346251413947. https://doi.org/10.1177/15347346251413947

Mariani, F., Costilla, C. R., Oppezzo, O. J., & Galvan, E. M. (2026). Combined Effects of Amikacin and Methylene Blue-Mediated Photodynamic Therapy on Pseudomonas aeruginosa Biofilms Mimicking Mono- and Polymicrobial Diabetic Foot Ulcer Infections. *Pathogens*, *15*(2). https://doi.org/10.3390/pathogens15020226

Meloni, M., Andreadi, A., Ruotolo, V., Romano, M., Bellizzi, E., Giurato, L., Bellia, A., Uccioli, L., & Lauro, D. (2026). Hospital Readmission in Patients With Diabetic Foot Ulcers: Prevalence, Causes, and Outcomes. *Int J Low Extrem Wounds*, *25*(1), 174-182. https://doi.org/10.1177/15347346231207747

Pinto, N. C. C., Silva, J. B., Menegati, L. M., Guedes, M., Marques, L. B., Silva, T. P. D., Melo, R. C. N., Souza-Fagundes, E. M., Salvador, M. J., Scio, E., & Fabri, R. L. (2017). Cytotoxicity and bacterial membrane destabilization induced by Annona squamosa L. extracts. *An Acad Bras Cienc*, *89*(3 Suppl), 2053-2073. https://doi.org/10.1590/0001-3765201720150702

Prasathkumar, M., & Sadhasivam, S. (2021). Chitosan/Hyaluronic acid/Alginate and an assorted polymers loaded with honey, plant, and marine compounds for progressive wound healing-Know-how. *Int J Biol Macromol*, *186*, 656-685. https://doi.org/10.1016/j.ijbiomac.2021.07.067

Račić, A., Krstonošić, V., Micov, A., Pecikoza, U., Dobričić, V., Turković, E., & Krajišnik, D. (2025). Stability and Efficacy of Mucoadhesive Eye Drops Containing Olopatadine HCl: Physicochemical, Functional, and Preclinical In Vivo Assessment. *Pharmaceutics*, *17*(4). https://doi.org/10.3390/pharmaceutics17040517

Ramadani, A. P., Syukri, Y., Hasanah, E., & Syahyeri, A. W. (2021). Acute Oral Toxicity Evaluation of Andrographolide Self-Nanoemulsifying Drug Delivery System (SNEDDS) Formulation. *J Pharm Bioallied Sci*, *13*(2), 199-204. https://doi.org/10.4103/jpbs.JPBS_267_19

Rizzo, M., Marussi, G., Crosera, M., Marcella, M., Biasiol, G., Adami, G., Magnano, G. C., & Larese Filon, F. (2025). Gallium and arsenic human skin permeation after application of GaAs particles: an ex-vivo study using Franz cells. *Food Chem Toxicol*, *206*, 115758. https://doi.org/10.1016/j.fct.2025.115758

Santos, E. D., Silva-Filho, S. E., Santos Radai, J. A., Arena, A. C., Fraga, T. L., Lima Cardoso, C. A., Croda, J., & Leite Kassuya, C. A. (2021). Anti-inflammatory properties of ethanolic extract from Vatairea macrocarpa leaves. *J Ethnopharmacol*, *278*, 114308. https://doi.org/10.1016/j.jep.2021.114308

Shrivastava, S., & Kaur, C. D. (2023). Development of andrographolide-loaded solid lipid nanoparticles for lymphatic targeting: Formulation, optimization, characterization, in vitro, and in vivo evaluation. *Drug Deliv Transl Res*, *13*(2), 658-674. https://doi.org/10.1007/s13346-022-01230-6

Somwong, P., & Theanphong, O. (2021). Quantitative analysis of triterpene lupeol and anti-inflammatory potential of the extracts of traditional pain-relieving medicinal plants Derris scandens, Albizia procera, and Diospyros rhodocalyx. *J Adv Pharm Technol Res*, *12*(2), 147-151. https://doi.org/10.4103/japtr.JAPTR_13_21

Talodthaisong, C., Patramanon, R., Thammawithan, S., Lapmanee, S., Maikaeo, L., Sricharoen, P., Khongkow, M., Namdee, K., Jantimaporn, A., Kayunkid, N., Hutchison, J. A., & Kulchat, S. (2023). A Shear-Thinning, Self-Healing, Dual-Cross Linked Hydrogel Based on Gelatin/Vanillin/Fe(3+) /AGP-AgNPs: Synthesis, Antibacterial, and Wound-Healing Assessment. *Macromol Biosci*, *23*(12), e2300250. https://doi.org/10.1002/mabi.202300250

Vikas, B., Anil, S., & Remani, P. (2019). Cytotoxicity Profiling of Annona Squamosa in Cancer Cell Lines. *Asian Pac J Cancer Prev*, *20*(9), 2831-2840. https://doi.org/10.31557/apjcp.2019.20.9.2831

Yang, G., Li, X., Li, Q., Xiao, C., Qian, H., Yang, H., & Shen, F. (2022). Andrographolide Suppresses Expressions of Coagulation and Fibrinolytic Inhibition-Related Factors in LPS-Induced Alveolar Epithelial Cell Type II via NF-κB Signal Pathway In Vitro. *Intensive Care Res*, *2*(3-4), 61-70. https://doi.org/10.1007/s44231-022-00010-7

Ye, P., Dai, Y., Zhang, Q., Yang, J., Liu, L., Guo, X., Zhu, H., Chen, J., Gu, R., Tan, M., Tang, M., Han, F., & Nie, X. (2026). Novel copper-ion coordinated andrographolide-loaded hydrogel activates Rac1/JNK1 axis for enhancing diabetic wound healing. *NPJ Regen Med*. https://doi.org/10.1038/s41536-026-00457-y

Yeh, S.-H., Chang, F.-R., Wu, Y.-C., Yang, Y.-L., Zhuo, S.-K., & Hwang, T.-L. (2005). An Anti-Inflammatory ent-Kaurane from the Stems of Annona squamosa that Inhibits Various Human Neutrophil Functions. *Planta Med*, *71*(10), 904-909. https://doi.org/10.1055/s-2005-871234

Youssef, M. M., El-Mansy, M. N., El-Borady, O. M., & Hegazy, E. M. (2021). Impact of biosynthesized silver nanoparticles cytotoxicity on dental pulp of albino rats (histological and immunohistochemical study). *J Oral Biol Craniofac Res*, *11*(3), 386-392. https://doi.org/10.1016/j.jobcr.2021.04.002

Yu, T., Jiang, X., Xu, X., Jiang, C., Kang, R., & Jiang, X. (2022). Andrographolide Inhibits Biofilm and Virulence in Listeria monocytogenes as a Quorum-Sensing Inhibitor. *Molecules*, *27*(10). https://doi.org/10.3390/molecules27103234

Yuan, X., Xu, W., Yan, Z., Xu, X., Chen, Y., Chen, S., & Wang, P. (2022). Andrographolide exerted anti-inflammatory effects thereby reducing sex hormone synthesis in LPS-induced female rats, but had no effect on hormone production in healthy ones. *Front Pharmacol*, *13*, 980064. https://doi.org/10.3389/fphar.2022.980064

Zhou, Y., Yang, M., Yan, X., Zhang, L., Lu, N., Ma, Y., Zhang, Y., Cui, M., Zhang, M., & Zhang, M. (2023). Oral Nanotherapeutics of Andrographolide/Carbon Monoxide Donor for Synergistically Anti-inflammatory and Pro-resolving Treatment of Ulcerative Colitis. *ACS Appl Mater Interfaces*, *15*(30), 36061-36075. https://doi.org/10.1021/acsami.3c09342

Zohmachhuana, A., Malsawmdawngliana, Lalnunmawia, F., Mathipi, V., Lalrinzuali, K., & Kumar, N. S. (2022). Curcuma aeruginosa Roxb. exhibits cytotoxicity in A-549 and HeLa cells by inducing apoptosis through caspase-dependent pathways. *Biomed*

Pharmacother, *150*, 113039. https://doi.org/10.1016/j.biopha.2022.113039